

Linear Tidal Vestige found in the WM Sheet

Jounghun Lee¹, Suk Kim², and Soo-Chang Rey³

ABSTRACT

We present a vestige of the linear tidal influence on the spin orientations of the constituent galaxies of the WM sheet discovered in the vicinity of the Virgo cluster and the Local Void. The WM sheet is chosen as an optimal target since it has a rectangular parallelepiped-like shape whose three sides are in parallel with the supergalactic Cartesian axes. Determining three probability density functions of the absolute values of the supergalactic Cartesian components of the spin vectors of the WM sheet galaxies, we investigate their alignments with the principal directions of the surrounding large-scale tidal field. When the WM sheet galaxies located in the central region within the distance of $2 h^{-1}\text{Mpc}$ are excluded, the spin vectors of the remaining WM sheet galaxies are found to be weakly aligned, strongly aligned, and strongly anti-aligned with the minor, intermediate and major principal directions of the surrounding large-scale tidal field, respectively. To examine whether or not the origin of the observed alignment tendency from the WM sheet is the linear tidal effect, we infer the eigenvalues of the linear tidal tensor from the axial ratios of the WM sheet with the help of the Zel'dovich approximation and conduct a full analytic evaluation of the prediction of the linear tidal torque model for the three probability density functions. A detailed comparison between the analytical and the observational results reveals a good quantitative agreement not only in the behaviors but also in the amplitudes of the three probability density functions.

Subject headings: cosmology — large scale structure of universe

¹Astronomy Program, Department of Physics and Astronomy, Seoul National University, Seoul 151-742, Korea

jounghun@astro.snu.ac.kr

²Korea Astronomy & Space Science institute, 776 Daedeokdae-ro, Daejeon 305-348, Korea

³Department of Astronomy and Space Science, Chungnam National University, Daejeon 305-764, Korea

1. Introduction

The anisotropic large-scale tidal field has an effect of producing a web-like pattern in the spatial distribution of the galaxies, which is often collectively referred to as the cosmic web (Bond et al. 1996). The voids, filaments, sheets and knots observed on the largest scales are the four constituent elements of the cosmic web and called the large-scale structures, whose formations are closely linked to the coherence of the principal directions of the large-scale tidal field (e.g., Hahn et al. 2007; Forero-Romero et al. 2009; Cautun et al. 2013). The three dimensional stretch (compression) of matter along three principal directions of the coherent large-scale tidal fields lead to the formation of voids (knots). The sheets (filaments) form at the boundaries between the voids through one (two) dimensional compression of matter only along the major (along the major and intermediate) principal directions (Zel’dovich 1970). The largest knots corresponding to the rich galaxy clusters in the universe often form at the intersections of the filaments along which the galaxies anisotropically merge with one another (West et al. 1995), while the smaller knots are mostly distributed along the filaments or embedded in the sheets.

Other than weaving the cosmic web, the linear tidal field has an effect of originating the spin angular momenta of the proto-galaxies. The linear tidal torque (LTT) model developed by Doroshkevich (1970) explains in the frame of the first-order Lagrangian perturbation theory that the exertion of the torque force of the linear tidal field causes an asymmetric proto-galactic region to possess the spin angular momentum (see also White 1984). The signature prediction of this LTT model is that the spin axes of the proto-galaxies tend to be strongly aligned, weakly aligned and strong antialigned with the intermediate, minor and major principal axes of the linear tidal tensors, respectively (Lee & Pen 2000, 2001; Porciani et al. 2002). In this model, the coherence in the principal directions of the linear tidal field is translated into that in the spin directions of the proto-galaxies.

Provided the linear tidal field can be well approximated by the large scale tidal field whose coherence is responsible for the formation of the cosmic web and that the spin axes of the present galaxies preserve well their initially induced tidal alignments, the effect of the linear tidal field on the spin directions of the proto-galaxies would be reflected at least to some degree by the alignments of the spin axes of the present galaxies with the shapes of the large-scale structures, since the eigenvectors of the inertia momentum tensors of the large-scale structures coincide well with the principal axes of the large-scale tidal field (Lee & Pen 2000; Porciani et al. 2002).

However, the spin directions of the galaxies after the turn-around moments are prone to severe nonlinear modifications especially during the compression and/or stretch of the surrounding matter distribution to form the large-scale structures. The N-body experiment

performed by Chen et al. (2016) demonstrated that only for the case of those large-scale structures that are still in the quasi-linear regime, it is possible to find a vestige of the linear tidal effect from the spin directions of the embedded galaxies. Another recent numerical study done by Brinckmann et al. (2016) showed that the galaxies embedded in the sheets have relatively low velocity dispersions compared with those in the filaments, which implied that the sheets are still in the quasi-linear regime, which is consistent with the numerical finding that the first objects ever condensed out are likely to have sheet-like shapes (Shandarin et al. 1995). Given these numerical results, we suggest that the galaxies embedded in the sheets are the best targets for the detection of the linear tidal effect on their spin axes.

Another merit of using the sheets is that the direction of at least the major principal axis of the surrounding large-scale tidal field can be relatively accurately determined (Navarro et al. 2004). For the case of a flat sheet, the major principal axis of the tidal field should be in the direction normal to the face of the sheet (called the sheet normal vector). For the case of a sheet wrapping a void, the radial vector from the center of a given void to a galaxy position in the void surface (void radial vector) must be in the direction of the major principal axis of the surrounding large-scale field. If a sheet truly preserved the initially imprinted memory of the linear tidal alignment at a detectable level, then the spin directions of the galaxies embedded in the sheet would show a tendency of being anti-aligned with the sheet normal vector (or equivalently, a tendency to lie in the plane of the sheet).

Several observational efforts were already made to dig up the linear tidal vestige from the sheet-like structures. For instance, Navarro et al. (2004) claimed that the anti-alignments of the spin axes of the local spiral galaxies belonging to the Local Supercluster with the direction of the supergalactic north pole should be taken as an evidence for the presence of the linear tidal vestige. Trujillo et al. (2006) investigated whether or not the spin axes of the spiral galaxies on the surfaces of the voids were anti-aligned with the void radial directions and claimed a detection of statistically significant signal. Hirv et al. (2017) noted that the origin and strength of the intrinsic spin alignments of the galaxies depend on the Hubble types of the galaxies, and showed that for the case of the Sab spiral galaxies located in the sheets, their spin directions show a tendency of anti-alignments with the sheet normal vector. These observational findings seemed quite consistent qualitatively with the trend predicted by the LTT model.

Yet, the presence of the linear tidal vestige in the sheets are still inconclusive, having been challenged by the recent reports of the counter evidences. Slosar & White (2009) re-investigated the spin directions of the galaxies at the void surfaces and found no signal of their anti-alignments with the void radial directions for the case of the spherical voids. Varela et al.

(2012) confirmed the finding of Slosar & White (2009) with a larger sample and claimed that the alignment tendencies show variation with the sizes of the voids. A similar counter evidence was also provided by Tempel & Libeskind (2013) who found no preferred directions in the orientations of the spin axes of the sheet galaxies, identifying the sheets using the "Biscous model". Given many numerical results that the spin axes of the galactic halos embedded in the sheets tend to be anti-aligned with the sheet normal vectors (e.g., Aragón-Calvo et al. 2007; Cuesta et al. 2008; Libeskind et al. 2013; Forero-Romero et al. 2014), those observational counter evidences may be interpreted not as real challenges but as an indication of the presence of systematics such as inaccurate measurements of the spin directions of the void galaxies, ambiguity and uncertainty involved with the identification of the voids and sheets, and so forth.

However, the previous works were inconclusive not only about the detection of the signal itself but also about the origin of the signal. The subsequent nonlinear evolution of the galaxies after the turn-around moments would not necessarily weaken but rather could strengthen the inclination of their spin axes to be aligned or anti-aligned with the shapes of the surrounding large-scale structures (Codis et al. 2012; Dubois et al. 2014; Welker et al. 2014; Laigle et al. 2015). To distinguish between the spin alignments originated by the linear tidal influences and those generated/strengthened by the nonlinear processes, what is required is an exact evaluation of the prediction of the LTT model on the spin alignments of the sheet galaxies and a detailed comparison of an observationally detected signal of the spin alignments with the prediction of the LTT model as well.

The linear tidal effect cannot produce an arbitrary high signal of the galaxy spin alignments but rather limits the strength of the signal. Only when the strength of an alignment signal from the galaxies embedded in a sheet is found to lie in the range constrained by the LTT model and the alignment tendencies agree quantitatively with the signature prediction of the LTT model as mentioned in the above, it can be declared as a detection of the linear tidal vestige from the sheet. In this paper, we aim at detecting the linear tidal vestige from a newly discovered sheet with a conspicuously rectangular parallelepiped shape.

We organize this paper to present the followings: A review of the LTT model and a full analytic derivation of its prediction on the spin directions of the sheet galaxies in Section 2. The results of testing the predictions of the LTT model against new observational data in Section 3. The summary of the final result and discussion of its implication as well as two caveats in Section 4.

2. A Review of the Linear Tidal Torque Model

2.1. Probability distributions of the unit galaxy spins

Suppose that a proto-galaxy located at a position \mathbf{r} has an angular momentum, \mathbf{J} , and that at the same position the linear tidal field $\mathbf{T} = (T_{ij})$ smoothed on the galactic mass scale has three distinct eigenvalues, $\{\lambda_1, \lambda_2, \lambda_3 | \lambda_1 \geq \lambda_2 \geq \lambda_3\}$. The linear tidal torque (LTT) theory relates \mathbf{J} to \mathbf{T} by modeling the conditional probability density function of \mathbf{J} given \mathbf{T} as the following multivariate Gaussian distribution (Catelan & Theuns 1996; Lee & Pen 2001; Porciani et al. 2002)

$$p(\mathbf{j}|\mathbf{T}) = p(J, \mathbf{j}|\mathbf{T}) = \frac{1}{[(2\pi)^3 \det(\mathbf{U})]^{1/2}} \exp \left[-\frac{J^2}{2} (\mathbf{j} \cdot \mathbf{U}^{-1} \cdot \mathbf{j}) \right]. \quad (1)$$

Here \mathbf{j} denotes the unit spin vector of a proto-galaxy defined as $\mathbf{j} \equiv \mathbf{J}/|\mathbf{J}|$, and $\det(\mathbf{U})$ is the determinant of the covariance matrix $\mathbf{U} = (U_{ij}) \equiv \langle j_i j_j | \mathbf{T} \rangle$ whose components are given as (Lee & Pen 2000, 2001)

$$U_{ij} = \frac{1 + c_t}{3} \delta_{ij} - c_t \sum_{k=1}^3 \hat{T}_{ik} \hat{T}_{kj}, \quad (2)$$

where $\hat{\mathbf{T}}$ is the unit traceless tidal shear tensor defined as $\hat{\mathbf{T}} \equiv \tilde{\mathbf{T}}/|\tilde{\mathbf{T}}|$ with $\tilde{\mathbf{T}} \equiv \mathbf{T} - (1/3) \sum_{i=1}^3 T_{ii}$, and c_t is a stochastic tidal link parameter that measures the strength of the correlation between \mathbf{j} and \mathbf{T} . The value of c_t depends on the degree of the misalignments between the principal axes of \mathbf{T} and those of the inertia momentum tensor, \mathbf{I} , of a proto-galaxy. The more misaligned they are with one another, the closer to unity the value of c_t can have (Lee & Pen 2000; Porciani et al. 2002).

Let $\hat{\mathbf{p}}_1$, $\hat{\mathbf{p}}_2$ and $\hat{\mathbf{p}}_3$ denote the major, intermediate and minor principal axes of \mathbf{T} , respectively (i.e., the orthonormal eigenvectors corresponding to λ_1 , λ_2 and λ_3 , respectively). In the principal axis frame of \mathbf{T} , the conditional probability density function of \mathbf{j} can be obtained by marginalizing Equation (1) over $J \equiv |\mathbf{J}|$ (Lee & Pen 2001):

$$\begin{aligned} p(\mathbf{j}|\mathbf{T}) &= \int p(\mathbf{j}|\mathbf{T}) J^2 dJ \\ &= \frac{1}{2\pi} \left[\left(1 + c_t - 3c_t \hat{\lambda}_1^2\right) \left(1 + c_t - 3c_t \hat{\lambda}_2^2\right) \left(1 + c_t - 3c_t \hat{\lambda}_3^2\right) \right]^{-\frac{1}{2}} \times \\ &\quad \left(\frac{|\hat{\mathbf{p}}_1 \cdot \mathbf{j}|}{1 + c_t - 3c_t \hat{\lambda}_1^2} + \frac{|\hat{\mathbf{p}}_2 \cdot \mathbf{j}|}{1 + c_t - 3c_t \hat{\lambda}_2^2} + \frac{|\hat{\mathbf{p}}_3 \cdot \mathbf{j}|}{1 + c_t - 3c_t \hat{\lambda}_3^2} \right)^{-\frac{3}{2}}, \end{aligned} \quad (3)$$

where $\hat{\lambda}_1$, λ_2 , λ_3 are the eigenvalues of $\hat{\mathbf{T}}$ distributed over a sphere with a radius of unity, satisfying the constraints of $\sum_{i=1}^3 \hat{\lambda}_i^2 = 1$ and $\sum_{i=1}^3 \hat{\lambda}_i = 0$ (Lee & Pen 2001).

The conditional probability density of the absolute value of the \mathbf{p}_i -axis component of \mathbf{j} (i.e, $|\hat{\mathbf{p}}_i \cdot \mathbf{j}|$) can be obtained as

$$p(|\hat{\mathbf{p}}_1 \cdot \mathbf{j}|) = \int_0^{2\pi} p(\mathbf{j}) d\phi_{23}, \quad p(|\hat{\mathbf{p}}_2 \cdot \mathbf{j}|) = \int_0^{2\pi} p(\mathbf{j}) d\phi_{31}, \quad p(|\hat{\mathbf{p}}_3 \cdot \mathbf{j}|) = \int_0^{2\pi} p(\mathbf{j}) d\phi_{12}, \quad (4)$$

where

$$\phi_{23} \equiv \tan^{-1} \left(\frac{\hat{\mathbf{p}}_2 \cdot \mathbf{j}}{\hat{\mathbf{p}}_3 \cdot \mathbf{j}} \right), \quad \phi_{31} \equiv \tan^{-1} \left(\frac{\hat{\mathbf{p}}_3 \cdot \mathbf{j}}{\hat{\mathbf{p}}_1 \cdot \mathbf{j}} \right), \quad \phi_{12} \equiv \tan^{-1} \left(\frac{\hat{\mathbf{p}}_1 \cdot \mathbf{j}}{\hat{\mathbf{p}}_2 \cdot \mathbf{j}} \right), \quad (5)$$

Equation (3) is not uniform provided that $c_t \neq 0$ and $\lambda_i \neq \lambda_j$ for $i, j \in \{1, 2, 3\}$. Depending on the sign of c_t , $p(\mathbf{j})$ behaves differently: for the case of $c_t > 0$, it yields

$$\langle |\hat{\mathbf{p}}_2 \cdot \mathbf{j}| \rangle > 0.5 \sim \langle |\hat{\mathbf{p}}_3 \cdot \mathbf{j}| \rangle > \langle |\hat{\mathbf{p}}_1 \cdot \mathbf{j}| \rangle, \quad (6)$$

which implies that the spin vectors of the proto-galaxies are strongly and weakly aligned with $\hat{\mathbf{p}}_2$ and $\hat{\mathbf{p}}_3$, respectively, but strongly anti-aligned with $\hat{\mathbf{p}}_1$. Whereas, for the case of $c_t < 0$, the inequality sign is reversed as

$$\langle |\hat{\mathbf{p}}_2 \cdot \mathbf{j}| \rangle < \langle |\hat{\mathbf{p}}_3 \cdot \mathbf{j}| \rangle \sim 0.5 < \langle |\hat{\mathbf{p}}_1 \cdot \mathbf{j}| \rangle. \quad (7)$$

The above unique prediction of the LTT model on the alignments between \mathbf{j} and \mathbf{T} is valid in the linear regime where the proto-galactic regions remain coupled to the surrounding linear tidal field before their turn-around moments. In the non-linear regime, the tidal field would develop non-Gaussianity on the galactic mass scale and the spin directions of the present galaxies would inevitably deviate from those of their progenitors. However, if some galaxies did not undergo severe nonlinear modifications in their spin orientations, the linear tidal influence on their spin directions would be manifested by their tendency of being aligned with the principal axes of the present large-scale tidal fields that can approximate the linear tidal field in the proto-galactic stage. In other words, Equations (4) and Equation (7) could be used to describe the alignments between the principal axes of the large-scale tidal fields and the spin axes of those present galaxies which have preserved well the initially induced tidal influences. From here on, we use \mathbf{T} to denote interchangeably both of the linear tidal field in the proto-galactic stage and the present large-scale tidal field, and \mathbf{j} to denote the spin axes of the present galaxies without confusing the readers.

Rearranging the terms of Equation (2), one can derive the following relation between the tidal link parameter c_t and the eigenvalues of $\hat{\mathbf{T}}$ (Lee & Pen 2000, 2001):

$$c_t = \frac{10}{3} - 3 \sum_{i=1}^3 |\hat{\lambda}_i|^2 |\hat{\mathbf{p}}_i \cdot \mathbf{j}|^2, \quad (8)$$

which implies that c_t would vary from realizations to realizations (or from galaxies to galaxies), since each realization would have a different degree of the misalignment between the principal axes of \mathbf{T} and \mathbf{I} .

Suppose that one has a sample of n_r galaxies with each having uniquely defined spin vector and that the eigenvalues and eigenvectors of the large-scale tidal tensor at the position of each galaxy are all specified. Applying Equation (8) to this sample will give n_r different values of c_t . The strength of the mean correlation between the spin vectors of the n_r galaxies and the eigenvectors of their surrounding tidal field will be determined by the ensemble average, $\langle c_t \rangle$, and its error, $\sigma_{c_t} = \sqrt{20/[9(n_r - 1)]}$ (Lee & Pen 2001). Provided that the values of \bar{c}_t , and $\{\hat{\lambda}_i\}_{i=1}^3$ are all specified, the LTT model will permit a fully analytical evaluation of the three probability density functions, $p(|\hat{\mathbf{p}}_1 \cdot \mathbf{j}|)$, $p(|\hat{\mathbf{p}}_2 \cdot \mathbf{j}|)$ and $p(|\hat{\mathbf{p}}_3 \cdot \mathbf{j}|)$ through Equations (1)-(4).

2.2. The galaxy spin alignments in the cosmic sheets

The tidal link parameter, c_t , depends not only on the position of a galaxy but also on the smoothing scale of \mathbf{T} . For a galaxy with mass M_g , the parameter c_t attains its maximum possible value when \mathbf{T} is smoothed on the same scale M_g , and decreases from the maximum value as the smoothing scale departs from M_g . However, if the tidal field possesses a large-scale coherence in the orientations of their principal axes, c_t would not substantially fluctuate with the variation of the smoothing scales. Even when \mathbf{T} is smoothed on a much larger mass scale than M_g , the correlation strength between \mathbf{j} and \mathbf{T} would not sharply decrease.

The coherence of \mathbf{T} often leads to a formation of the large-scale structure whose constituent galaxies exhibit highly anisotropic spatial distributions. Both of a sheet and a filament are the most representative large-scale structures that reflects the coherence in the principal directions of \mathbf{T} . Between the two, however, it is only the sheet that still remains in the quasi-linear regime (Chen et al. 2016). The simplest theory with highest efficacy to describe the formation of a cosmic sheet is the Zel'dovich approximation, according to which the ratio of the present to the initial matter density, $\rho/\bar{\rho}$, at a given region is expressed in terms of three eigenvalues of \mathbf{T} as (Zel'dovich 1970):

$$\frac{\rho}{\bar{\rho}} = \frac{1}{(1 - \lambda_1)(1 - \lambda_2)(1 - \lambda_3)}. \quad (9)$$

Equation (9) carries two crucial implications: First, a cosmic sheet forms through the compression of matter along $\hat{\mathbf{p}}_1$ at a region where λ_1 comes close to unity when \mathbf{T} is smoothed on the sheet scale. The fate of a sheet depends on the signs of the other two eigenvalues. If

λ_2 and λ_3 are negative when $\lambda_1 \sim 1$, then the matter in the sheet would never compress along the other two principal axes, retaining its two dimensional sheet-like shape for ever. The great wall and the sloan wall must fall into this category (Geller & Huchra 1989; Gott et al. 2005). In contrast, for the case of $\lambda_2 \geq \lambda_3 \geq 0$, then the region will first evolve into a sheet via the one dimensional compression along $\hat{\mathbf{p}}_1$. However, in the subsequent process, it will also collapse along $\hat{\mathbf{p}}_2$ and $\hat{\mathbf{p}}_3$ to evolve into a filament and eventually into a knot, respectively. Lee (2004) defined a cosmic sheet of the second type as a structure that forms at a region where the smallest tidal eigenvalue, λ_3 , just reaches zero. To justify this definition, Lee (2004) computed the expectation value of λ_1 under the condition of $\lambda_3 = 0$ and found $\langle \lambda_1 | \lambda_3 \rangle \sim 0.9$ (i.e., the condition for the one dimensional collapse along $\hat{\mathbf{p}}_1$ according to the Zel'dovich approximation), regardless of the smoothing scale.

It is worth mentioning why the definition of a sheet suggested by Lee (2004) and adopted here seems apparently different from the the conventional one according to which a sheet corresponds to a region where the local tidal tensor smoothed on a certain scale has only one positive eigenvalue (e.g., Hahn et al. 2007; Zhang et al. 2015). The difference lies in the fact that the eigenvalues in the two definitions are not the same ones. In the latter the eigenvalues are the Eulerian quantities describing the matter distribution surrounding a sheet after its formation via the one dimensional compression, while in the latter the eigenvalues, i.e., $\{\lambda_i\}_{i=1}^3$, that appear in Equations (3)-(9) are not the Eulerian but the Lagrangian quantities describing the surrounding matter distribution before the formation of a sheet.

Combining the condition of $\lambda_3 = 0$ with the other two constraints of $\sum \hat{\lambda}_i^2 = 1$ and $\sum \hat{\lambda}_i = 0$, one can show that $\{\hat{\lambda}_i\}_{i=1}^3$ can be written in terms only of λ_1 and λ_2 as (Lee 2004):

$$\hat{\lambda}_1 = \frac{2\lambda_1 - \lambda_2}{\sqrt{6(\lambda_1^2 - \lambda_1\lambda_2 + \lambda_2^2)}}, \quad (10)$$

$$\hat{\lambda}_2 = \max \left\{ \frac{2\lambda_2 - \lambda_1}{\sqrt{6(\lambda_1^2 - \lambda_1\lambda_2 + \lambda_2^2)}}, \frac{-(\lambda_1 + \lambda_2)}{\sqrt{6(\lambda_1^2 - \lambda_1\lambda_2 + \lambda_2^2)}} \right\}, \quad (11)$$

$$\hat{\lambda}_3 = \min \left\{ \frac{2\lambda_2 - \lambda_1}{\sqrt{6(\lambda_1^2 - \lambda_1\lambda_2 + \lambda_2^2)}}, \frac{-(\lambda_1 + \lambda_2)}{\sqrt{6(\lambda_1^2 - \lambda_1\lambda_2 + \lambda_2^2)}} \right\}. \quad (12)$$

The second implication of Equation (9) is that the observed shape of a cosmic sheet can be used to determine the eigenvalues of the surrounding large-scale tidal field. Suppose that a sheet has a shape of a rectangular parallelepiped with side lengths L_1, L_2, L_3 with $L_1 \geq L_2 \geq L_3$. The longest, second longest and shortest sides of this parallelepiped-like sheet must be in parallel to the minor ($\hat{\mathbf{p}}_3$), intermediate ($\hat{\mathbf{p}}_2$) and major ($\hat{\mathbf{p}}_1$) principal axes of \mathbf{T} , respectively, with its present volume given as $V_{\text{sheet}} = \prod_{i=1}^3 L_i$. Let V_L denote the volume of

a cosmic sheet in its initial stage before the completion of the gravitational collapse along $\hat{\mathbf{p}}_1$ where the matter density of the sheet equals the mean background density. Since the mass contained in a volume is always conserved, one can say $\rho V_{\text{sheet}} = \rho \prod_{i=1}^3 L_i = \bar{\rho} V_L$. By Equation (9), we now have the following relation between $\{L_i\}_{i=1}^3$ and $\{\lambda_i\}_{i=1}^3$

$$L_1 = V_L^{1/3}(1 - \lambda_3), \quad L_2 = V_L^{1/3}(1 - \lambda_2), \quad L_3 = V_L^{1/3}(1 - \lambda_1). \quad (13)$$

Putting $\lambda_3 = 0$ (the sheet criterion) into Equation (13), one can determine the value of the proportionality constant, $V_L^{1/3}$. Putting the determined value of $V_L^{1/3}$ back into Equation (13), one can obtain the values of λ_2 and λ_1 , which can in turn be used to find the values of $\{\hat{\lambda}_i\}_{i=1}^3$ through Equations (10)-(12) and the value of c_t by Equation (8). Finally, a complete analytic evaluation of the prediction of the LTT model on the intrinsic spin alignments of the galaxies embedded in a cosmic sheet can be made by putting $\{\hat{\lambda}_i\}_{i=1}^3$ and \bar{c}_t into Equation (4), where \bar{c}_t is the average of c_t taken over the constituent galaxies of the sheet.

3. Testing the LTT model with the WM Sheet

The WM sheet is a sheet-like structure composed of 204 galaxies (called the WMs galaxies hereafter ¹) discovered by Kim et al. (2016) in the vicinity of the Virgo cluster and the Local Void (see Figures 1 and 2 in Kim et al. 2016). The ranges of the supergalactic Cartesian coordinates, (x_{sg}, y_{sg}, z_{sg}) of the WMs galaxies are listed in Table 1. Although it is located in the neighborhood of the Virgo cluster, a careful analysis of the recession velocities of the WMs galaxies has revealed that the WM sheet does not gravitationally interact with the Virgo cluster (Kim et al. 2016).

The top-left, top-right and bottom-left panels of Figure 1 show the projected positions of the WMs galaxies onto the supergalactic $\hat{\mathbf{x}}\text{-}\hat{\mathbf{y}}$, $\hat{\mathbf{y}}\text{-}\hat{\mathbf{z}}$ and $\hat{\mathbf{x}}\text{-}\hat{\mathbf{z}}$ planes, respectively. As can be seen, the WM sheet has an interesting property: its shape is well approximated as a rectangular parallelepiped with its longest, second longest, and shortest sides well aligned the supergalactic $\hat{\mathbf{x}}$, $\hat{\mathbf{y}}$ and $\hat{\mathbf{z}}$ axes, respectively. Given this observed property of the WM sheet the principal axes of the surrounding large-scale tidal field seem to coincide with the supergalactic Cartesian axes as: $\hat{\mathbf{p}}_1 \parallel \hat{\mathbf{z}}$, $\hat{\mathbf{p}}_2 \parallel \hat{\mathbf{y}}$, $\hat{\mathbf{p}}_3 \parallel \hat{\mathbf{x}}$, since the shortest and longest sides of a sheet are expected to be aligned with the directions of the strongest and the weakest tidal forces.

¹Kim et al. (2016) found that the WM sheet comprise a total of 220 galaxies. However, information on the position angle and axial ratios are available only for 204 WMs galaxies.

Extracting information on the position angles (ψ) and axial ratios (R_{axial}) of the WMs galaxies obtained through the sersic fitting from the website of the NASA-Sloan-Atlas galaxy catalog ², we adopt the conventional methodology to determine the unit spin vector of each WMs galaxy in the equatorial Cartesian coordinate system as (Lee & Pen 2000; Pen et al. 2000; Trujillo et al. 2006; Lee 2011; Varela et al. 2012; Tempel et al. 2013)

$$\begin{pmatrix} j_x \\ j_y \\ j_z \end{pmatrix}_{\text{equatorial}} = \begin{pmatrix} j_r \sin \theta \cos \phi + j_\theta \cos \theta \cos \phi - j_\phi \sin \phi \\ j_r \sin \theta \sin \phi + j_\theta \cos \theta \sin \phi + j_\phi \cos \phi \\ j_r \cos \theta - j_\theta \sin \theta \end{pmatrix}, \quad (14)$$

where the spherical polar components of the unit spin vector, j_r , j_θ , j_ϕ , are given in terms of R_{axis} and ψ as

$$j_r = \pm R_{\text{axial}}, \quad j_\theta = \sqrt{1 - \cos^2 \xi} \sin \psi, \quad j_\phi = \sqrt{1 - \cos^2 \xi} \cos \psi. \quad (15)$$

The plus and minus signs before R_{axial} indicate our inability to determine whether the rotation of a WMs galaxy upon its spin axis is clock or counterclock wise. This two-fold sign ambiguity in the determination of \mathbf{j} increases the total number of the realizations of \mathbf{j} to twice the total number of the WMs galaxies. That is, we have a total of 408 realizations of \mathbf{j} from the WM sheet.

The unit spin vector \mathbf{j} in the supergalactic Cartesian coordinate system can be obtained through the rotation of the coordinate system as

$$\begin{pmatrix} j_x \\ j_y \\ j_z \end{pmatrix}_{\text{supergalactic}} = \begin{pmatrix} R_{11} & R_{12} & R_{13} \\ R_{21} & R_{22} & R_{23} \\ R_{31} & R_{32} & R_{33} \end{pmatrix}^{-1} \begin{pmatrix} j_x \\ j_y \\ j_z \end{pmatrix}_{\text{equatorial}} \quad (16)$$

where \mathbf{R}^{-1} is the inverse (or transponse) of the rotation matrix $\mathbf{R} = (R_{ij})$ whose nine components can be obtained from the J2000 values of the right ascension and declination of the supergalactic North pole ($\alpha_n = 2.82 \text{ h}$, $\delta_n = +59.5^\circ$) and those of the supergalactic zero point line ($\alpha_0 = 2.82 \text{ h}$, $\delta_0 = +59.5^\circ$):

$$(R_{ij}) = \begin{pmatrix} \cos \delta_0 \cos \alpha_0 & \sin \delta_n \cos \alpha_n \sin \alpha_0 - \sin \alpha_n \sin \delta_0 \cos \alpha_0 & \cos \delta_n \cos \alpha_n \\ \sin \delta_0 \cos \alpha_0 & \sin \alpha_n \cos \delta_0 \cos \alpha_0 - \cos \delta_n \cos \alpha_n \sin \alpha_0 & \sin \delta_n \cos \alpha_n \\ \sin \alpha_0 & \cos \alpha_n \cos \alpha_0 \sin(\delta_0 - \delta_n) & \sin \alpha_n \end{pmatrix}. \quad (17)$$

From here on, $\mathbf{j} = (j_x, j_y, j_z)$ denote exclusively the spin vector of a WMs galaxy measured in the supergalactic Cartesian coordinate system.

²<http://www.nsatlas.org/data>

The absolute value of the $\hat{\mathbf{x}}$ -axis component of \mathbf{j} , $|j_x|$, is in the range of $[0, 1]$. Breaking this unit interval into four bins of equal size $1/4$, we count the number of the realizations falling in each bin to determine in a discrete way the probability density function of $|j_x|$ as $p(|j_x|_i) = 4n_i/N_r$ where $|j_x|_i$ and n_i are the value of $|j_x|$ and the number of the realizations at the i -th bin, respectively, and N_r is the total number of the realizations. The errors are estimated by employing the Bootstrap method as

$$\sigma_{x,i}^2 = \frac{1}{N_{\text{boot}}} \sum_{k=1}^{N_{\text{boot}}} [p^k(|j_x|_i) - p(|j_x|_i)]^2, \quad (18)$$

where $\sigma_{x,i}$ is the error in the measurement of $p(|j_x|_i)$ at the i -th bin, $N_{\text{boot}} = 10000$ is the number of the Bootstrap resamples, and $p^k(|j_x|_i)$ is the probability density at the i -th bin from the k -th Bootstrap resample. The other two probability density functions, $p(|j_y|)$ and $p(|j_z|)$, along with their errors are all determined in the same manner.

The top-left, top-middle and top-right panels of Figure 2 show this observationally determined probability density functions, $p(|j_x|)$, $p(|j_y|)$ and $p(|j_z|)$, respectively, as filled black circles with the Bootstrap errors. Since $\hat{\mathbf{x}} \parallel \hat{\mathbf{p}}_3$, $\hat{\mathbf{y}} \parallel \hat{\mathbf{p}}_2$, $\hat{\mathbf{z}} \parallel \hat{\mathbf{p}}_1$, the observational results shown in Figure 2 are in fact the probability density functions of the absolute values of the components of the unit spin vectors of the WMs galaxies along the minor, intermediate and major principal axes of the surrounding large-scale tidal field, respectively. That is, $p(|j_x|) = p(|\hat{\mathbf{p}}_3 \cdot \mathbf{j}|)$, $p(|j_y|) = p(|\hat{\mathbf{p}}_2 \cdot \mathbf{j}|)$ and $p(|j_z|) = p(|\hat{\mathbf{p}}_1 \cdot \mathbf{j}|)$.

As can be seen in Figure 2, $p(|j_x|)$ appears to be more or less uniform. No consistent trend of increment nor decrement with $|j_z|$ is found in the shape of $p(|j_z|)$, either. But, its abrupt deep drop at the fourth bin from the right implies that it is less probable to find the WMs galaxies whose spin vectors are aligned with the major principal axis of the surrounding tidal field. Meanwhile, a clear signal of the preferential alignment of \mathbf{j} with $\hat{\mathbf{p}}_2$ is found in the shape of $p(|j_y|)$, which seems qualitatively consistent with the prediction of the LTT model.

The bottom panels of Figure 2 show the corresponding number distributions of the realizations of the spin axes of the WM galaxies as histograms with the Poisson errors. Strictly speaking, both of the bootstrap and Poisson errors are the underestimation of the true uncertainties associated with the measurements of the probability density or equivalently the number distributions. It is because the two realizations of the spin axis of each WM galaxy are not independent with each other but differs from each other only in the sign of j_r , while the bootstrap and Poisson errors have been estimated under the assumption that the two realizations are mutually independent. However, it does not necessarily mean that the true uncertainties should be larger than the Poisson errors by a factor of $\sqrt{2}$. Although

the two realizations are correlated with each other, their orientations with respect to the principal directions of the linear tidal field could be quite different from each other. The true spin axis of each WM galaxy is either one of the two realizations. If one realization is the real spin axis being aligned with the principal direction of the linear tidal field, then the other realization that has an opposite sign in j_r is likely to have no tidal alignment tendency. This is why the previous works that statistically investigated the tidal alignments of the galaxy spin axes (e.g., Pen et al. 2000; Varela et al. 2012; Tempel & Libeskind 2013) adopted the assumption that the two realizations are mutually independent. As a matter of fact, Varela et al. (2012) justified this assumption with the help of a Monte-carlo simulation.

Now that $p(|j_x|)$, $p(|j_y|)$, $p(|j_z|)$ are all observationally determined, we would like to make a quantitative comparison of them with the prediction of the LTT model. Taking the differences between the maximum and minimum values of the supergalactic Cartesian coordinates of each WMs galaxies (see Table 1), we measure the side lengths of the WM sheet as

$$L_3 = (x_{\text{sg,max}} - x_{\text{sg,min}}), \quad L_2 = (y_{\text{sg,max}} - y_{\text{sg,min}}), \quad L_1 = (z_{\text{sg,max}} - z_{\text{sg,min}}), \quad (19)$$

which gives $L_3 = 11.22$ Mpc, $L_2 = 8.95$ Mpc, and $L_1 = 1.32$ Mpc. Plugging these values as well as the sheet-condition of $\lambda_3 = 0$ into Equation (13), we find $\lambda_1 = 0.88$, $\lambda_2 = 0.2$ and $V_L^{1/3} = 11.21$ Mpc. Putting the values of λ_1 and λ_2 into Equations (10)-(12), we finally draw $\hat{\lambda}_1 = 0.797$, $\hat{\lambda}_2 = -0.243$ and $\hat{\lambda}_3 = -0.553$.

Plugging the measured values of $\{\hat{\lambda}_i\}_{i=1}^3$ along with the three components of the unit spin vectors into Equation (8), we finally determine the 408 different values of c_t for the same number of the \mathbf{j} -realizations. The top left panel of Figure 3 displays the probability density function of c_t , which seems to reach its maximum around $c_t = 0.1$, exhibiting a widely spread asymmetric shape over the range of $[-3, 3]$. The first row of Table 2 lists the mean value, \bar{c}_t , averaged over the 408 realizations and its associated error σ_{c_t} , revealing a detection of a statistically significant signal of the correlation between \mathbf{j} and $\hat{\mathbf{T}}$ from the WM sheet.

Putting the measured values of $\{\hat{\lambda}_i\}_{i=1}^3$ and \bar{c}_t into Equations (3)-(4), we analytically evaluate the probability density functions of the components of the unit spin vectors of the WMs galaxies along the major, intermediate and minor principal axes of the surrounding large-scale tidal field. which are displayed as green area in Figure 2. Recalling that $|j_x| = |\hat{\mathbf{p}}_3 \cdot \mathbf{j}|$, $|j_y| = |\hat{\mathbf{p}}_2 \cdot \mathbf{j}|$, $|j_z| = |\hat{\mathbf{p}}_1 \cdot \mathbf{j}|$, we note that the observational results (filled circular dots) do not agree with the analytic prediction (green area) at the quantitatively level.

We suspect that this failure of the LTT model in quantitatively matching the observational results should be caused by the development of the non-linearity in the dense inner region of the WM sheet. The LTT model which assumes the Gaussianity of $p(\mathbf{j})$ is strictly valid only in

the linear regime where the matter density rms fluctuation does not exceeds unity. Equation (2) which measures the covariance among the components of the unit spin vectors of the galaxies is also strictly effective only in the linear regime (Lee & Pen 2008). Furthermore, the Zel’dovich approximation from which the sheet-criterion of $\lambda_3 = 0$ is extracted also breaks down in the nonlinear regime (Shandarin 1994).

In the top-left panel of Figure 1, one can glimpse of the presence of a filament-like substructure aligned with the supergalactic $\hat{\mathbf{y}}$ -axis in the inner section of the WM sheet, which actually indicates that the inner overdense section of the WM sheet may have already begun gravitational collapse along $\hat{\mathbf{p}}_2$, entering a nonlinear regime. To eliminate the contamination caused by the existence of this nonlinear substructure, we first find the center of the WMs galaxies, say $\mathbf{x}_{sg,c}$, $\mathbf{y}_{sg,c}$, $\mathbf{z}_{sg,c}$. Then, we measure the distance vector, $\mathbf{d} = (d_x, d_y, d_z)$, of each WMs galaxy from the center as $d_x = |x_{sg} - x_{sg,c}|$, $d_y = |y_{sg} - y_{sg,c}|$, $d_z = |z_{sg} - z_{sg,c}|$. Then, we repeat the whole analysis with only those WMs galaxies that satisfy $d_x \geq d_{x,c}$ where $d_{x,c} \sim 1.2$ Mpc is the median value of the $\hat{\mathbf{x}}$ -axis components of the distance vectors of the WMs galaxies. The left panel of Figure 4 shows the configurations of the WM galaxies satisfying the condition of $d_x \geq d_{x,c}$ as filled red dots in the supergalactic plane.

The top-right panel of Figure 3 plots the same as the top-left but for the case of only those WMs galaxies with $d_x \geq d_{x,c}$. The c_t -distribution exhibits a more asymmetric shape, being biased toward the positive values of c_t . Figure 5 displays the same as Figure 2 but for this case of $d_x \geq d_{x,c}$. As can be seen, although the mean value of c_t for this case (listed in the second row of Table 2) is found to decrease, the three probability density functions, $p(|j_x|)$, $p(|j_y|)$, $p(|j_z|)$, show much better agreements with the analytic prediction of the LTT theory.

Repeating the whole calculations with those WMs galaxies that satisfy $d_x < d_{x,c}$, we show the corresponding results in the bottom left panel of Figure 3, Figure 6 and third row of Table 2. As can be seen, although the alignment tendency between \mathbf{j} and $\hat{\mathbf{p}}_2$ becomes stronger, the overall agreements between the observational and the analytical probability density functions degrade significantly. Especially, the weak \mathbf{j} - $\hat{\mathbf{p}}_2$ alignment and the strong \mathbf{j} - $\hat{\mathbf{p}}_1$ anti-alignments predicted by the LTT model seem to disappear in this observational result for the case of $d_x < d_{x,c}$.

Noting that the exclusion of the inner dense section from the WM sheet is important for the detection of a true linear tidal vestige, we measure the distance of each WM galaxy from the center as $d = \sqrt{d_x^2 + d_y^2 + d_z^2}$ and redo the analysis with those WMs galaxies satisfying $d \geq d_c \sim 2.2$ Mpc, where d_c represents a typical nonlinear scale. The right panel of Figure 4 shows the 2D configuration of these WM galaxies with $d \geq d_c$ in the supergalactic plane as filled red dots. The bottom-right panel of Figure 3, Figure 7 and the fourth row of

Table 2 show the corresponding results of this reanalysis. As can be seen, the exclusion of $d < d_c$ yields even a better quantitative agreement between the observational and the analytic results than that for the case of $d_x \geq d_{x,c}$. The mean parameter, \bar{c}_t , turns out to increase up to 0.29 ± 0.01 , confirming that the linear tidal vestige remains in the WM sheet at a statistically significant level.

It is worth discussing why the WM galaxies with $d \geq d_c$ yield a stronger signal of the linear tidal alignment than those with $d_x \geq d_{x,c}$, even though the substantial fraction of the WM galaxies with $d \geq d_c$ obviously belong to the filamentary section defined as $d_x < d_{x,c}$ (see Figure 4). Although the WM sheet as a whole is a quasi-linear structure, its densest core enclosed by d_c is believed to have undergone a severe nonlinear evolution. In consequence the spin directions of the WM galaxies located in the central core section with $d < d_c$ must have almost completely lost their initial tendency of being aligned with the principal directions of the linear tidal field. The section with $d \geq d_c$ does not contain those WM galaxies whose spin directions have lost their memory of the linear tidal effect, while the section with $d_x \geq d_{x,c}$ contains such galaxies, which explains why the former yields a better agreement with the analytic prediction of the LTT model than the latter. Our results shown in Figures 5-7 imply that the nonlinear effect on the spin directions of the WM galaxies in the filament section with $d_x < d_{x,c}$ would not be so strong as those in the central core section with $d \geq d_c$.

4. Summary and Discussion

We have tested the LTT (linear tidal torque) model against the WM sheet whose longest, second longest, and shortest sides are observed to be parallel with the supergalactic Cartesian $\hat{\mathbf{x}}$, $\hat{\mathbf{y}}$ and $\hat{\mathbf{z}}$ axes, respectively (Figure 1). Measuring the unit spin vectors, $\mathbf{j} = (j_x, j_y, j_z)$, of the WMs galaxies (WM sheet galaxies) in the supergalactic coordinate system according to the conventional methodology, we have determined in a discrete way three probability density functions, $p(|j_x|)$, $p(|j_y|)$, $p(|j_z|)$, and found a sharp increase of $p(|j_y|)$ with $|j_y|$, an abrupt deep drop of $p(|j_z|)$ below unity at $|j_z| \sim 1$, and no consistent variation of $p(|j_x|) \sim 1$ against $|j_x|$ (Figure 2).

Noting that the minor ($\hat{\mathbf{p}}_3$), intermediate ($\hat{\mathbf{p}}_2$) and major ($\hat{\mathbf{p}}_1$) principal directions of the large-scale tidal field surrounding the WM sheet coincide with the supergalactic $\hat{\mathbf{x}}$, $\hat{\mathbf{y}}$ and $\hat{\mathbf{z}}$ axes, respectively, we have interpreted this observational result as a supporting evidence for the existence of the strong alignment and anti-alignment of \mathbf{j} with $\hat{\mathbf{p}}_2$ and $\hat{\mathbf{p}}_1$, which trend is consistent with the prediction of the LTT model (Lee & Pen 2000, 2001), under the well justified assumption that the large-scale tidal field surrounding the WM sheet is a good approximation to the linear tidal field coherent over the mass scale of the WM sheet.

Measuring the side lengths of the WM sheet and assuming that the smallest eigenvalue of the linear tidal tensor at the center of the WM sheet is zero (Lee 2004), we have determined the other two (largest and second largest) tidal eigenvalues with the help of the Zel’dovich approximation (Zel’dovich 1970). Then, we have measured the mean values of the tidal link parameter, \bar{c}_t , which quantifies the degree of the deviations of the above three probability density functions from the uniform distribution. The obtained values of λ_1 , λ_2 , c_t have allowed us to evaluate $p(|j_x|)$, $p(|j_y|)$, $p(|j_z|)$ in a full analytic manner according to the LTT model.

The analytic predictions of the LTT model have failed in matching quantitatively the observed behaviors of the three probability density functions. Suspecting that the growth of nonlinearity in the inner denser section of the WM sheet should be responsible for this failure of the LTT model, we have excluded those WMs galaxies located in the central core of a typical nonlinear scale radius and redone the whole analysis. All of the three probability density functions, $p(|j_x|)$, $p(|j_y|)$, $p(|j_z|)$, from this reanalysis have been shown to agree quantitatively well with the analytic predictions of the LTT model in their shapes and amplitudes (Figure 7).

The previous works which attempted to observationally test the LTT model using the sheet galaxies focused only on the anti-alignments between \mathbf{j} and $\hat{\mathbf{p}}_1$ (or equivalently the tendency of \mathbf{j} lying on the planes of the sheets) and measured the correlation strength between \mathbf{j} and $\hat{\mathbf{p}}_1$ through fitting the observationally obtained $p(|j_z|)$ to an empirically constructed formula (e.g., Trujillo et al. 2006; Slosar & White 2009; Varela et al. 2012). However, the detection of a signal of the \mathbf{j} - $\hat{\mathbf{p}}_1$ anti-alignment and the agreement of the observational result with the fitting formula do not suffice to declare a discovery of the linear tidal vestige, no matter how strong the signal is and no matter how well the agreement turns out to be. This is because the other nonlinear processes could contribute to the presence of strong \mathbf{j} - $\hat{\mathbf{p}}_1$ anti-alignment (e.g., Lee & Pen 2008; Codis et al. 2012; Dubois et al. 2014; Welker et al. 2014; Laigle et al. 2015). Besides, the LTT model does not predict an arbitrary high signal of the \mathbf{j} - $\hat{\mathbf{p}}_1$ anti-alignment but rather puts an upper limit on the strength of the signal (or equivalently, on the possible values of the tidal correlation parameter c_t). In the current work, even though we have derived the three probability density functions, $p(|j_x|)$, $p(|j_y|)$, $p(|j_z|)$, purely from the linear physics, without resorting to any empirical formula or to fitting procedure, we still witness good quantitative agreements of them with the observational results from the WMs galaxies.

Another merit of our analysis is that we have been able to determine the eigenvalues and eigenvectors of the linear tidal tensor at the location of the WM sheet without resorting to a noisy reconstruction of the whole tidal field, owing to the particularly regular parallelepiped-

like shape of the WM sheet. In the previous approaches to the detection of the large-scale tidal effects on the directions of the galaxy angular momenta (e.g., Lee & Erdogdu 2007; Zhang et al. 2015), the whole tidal field had to be reconstructed, which could be, however, quite noisy, depending on the background cosmology, and introducing an additional free parameter, the smoothing scale.

Before drawing a conclusion, however, we would like to discuss two caveats. First, we have inferred the eigenvalues of the large-scale tidal field surrounding the WM sheet from the measurements of its three side lengths (L_1 , L_2 , L_3) under the assumption that the spatial extent of the distribution of the WMs galaxies observed in redshift space is at least proportional to that of the underlying dark matter in real space. Although recent numerical simulations showed that the sheets are in the quasi-linear regime containing very few nonlinear objects (Chen et al. 2016; Cautun et al. 2014), this assumption has to be justified with a hydrodynamic simulation.

Second, we have implicitly assumed that the spin axis directions of the WMs galaxies are perfectly aligned with those of the underlying dark matter halos, when we adopted the conventional methodology to measure the spin directions of the WMs galaxies. The validity of this assumption, however, is rather limited given the results of the recent hydrodynamic simulations that the spin axes of the stellar parts of the galaxies are aligned not with those of the entire galactic halos but with those of the core parts of the halos (e.g., Hahn et al. 2010; Varela et al. 2012; Tenneti et al. 2014; Zjupa & Springel 2017). Yet, these hydrodynamic results do not necessarily indicate that the observed alignments of the galaxy spin axes have no tidal origin. In fact, the angular momenta of the stellar parts of the galaxies could develop even stronger correlations with the linear tidal field and may preserve better the initial tidal memory since the spin axes of the inner regions of the halos should be least affected by the external nonlinear processes and thus may not undergo severe modifications in the subsequent evolution.

Our future work is in the direction of investigating the above issues with a hydrodynamic simulations: how the ratios of the side lengths of the luminous parts of the sheets are related to those of the underlying dark matter distribution; how strongly the spin axes of the stellar parts of the galaxies are aligned with the linear tidal field compared with their dark halo counterparts. With these caveats, it is concluded that our result supports compellingly the LTT model and that the vestige of the linear tidal influences on the galaxy angular momenta are best preserved in the sheet environments.

We are grateful to an anonymous referee for very useful comments. This work was supported by a research grant from the National Research Foundation (NRF) of Korea to

the Center for Galaxy Evolution Research (No.2017R1A5A1070354). J.L. was also partially supported by the Basic Science Research Program through the NRF of Korea funded by the Ministry of Education (NO. 2016R1D1A1A09918491). S.C.R was also partially supported by the Basic Science Research Program through the NRF of Korea funded by the Ministry of Education (No. 2015R1A2A2A01006828 and 2018R1A2B2006445).

REFERENCES

- Aragón-Calvo, M. A., van de Weygaert, R., Jones, B. J. T., & van der Hulst, J. M. 2007, *ApJ*, 655, L5
- Cautun, M., van de Weygaert, R., & Jones, B. J. T. 2013, *MNRAS*, 429, 1286
- Cautun, M., van de Weygaert, R., Jones, B. J. T., & Frenk, C. S. 2014, *MNRAS*, 441, 2923
- Bett, P. E., & Frenk, C. S. 2016, *MNRAS*, 461, 1338
- Bland-Hawthorn, J., & Peebles, P. J. E. 2006, *Science*, 313, 311
- Bond, J. R., Kofman, L., & Pogosyan, D. 1996, *Nature*, 380, 603
- Brinckmann, T., Lindholmer, M., Hansen, S., & Falco, M. 2016, *JCAP*, 4, 007
- Catelan, P., & Theuns, T. 1996, *MNRAS*, 282, 436
- Chen, S., Wang, H., Mo, H. J., & Shi, J. 2016, *ApJ*, 825, 49
- Codis, S., Pichon, C., Devriendt, J., et al. 2012, *MNRAS*, 427, 3320
- Cuesta, A. J., Betancort-Rijo, J. E., Gottlöber, S., et al. 2008, *MNRAS*, 385, 867
- Doroshkevich, A. G. 1970, *Astrofizika*, 6, 581
- Dubinski, J. 1992, *ApJ*, 401, 441
- Dubois, Y., Pichon, C., Welker, C., et al. 2014, *MNRAS*, 444, 1453
- Forero-Romero, J. E., Hoffman, Y., Gottlöber, S., Klypin, A., & Yepes, G. 2009, *MNRAS*, 396, 1815
- Forero-Romero, J. E., Contreras, S., & Padilla, N. 2014, *MNRAS*, 443, 1090
- Geller, M. J., & Huchra, J. P. 1989, *Science*, 246, 897
- Gott, J. R., III, & Thuan, T. X. 1978, *ApJ*, 223, 426
- Gott, J. R., III, Jurić, M., Schlegel, D., et al. 2005, *ApJ*, 624, 463
- Hahn, O., Porciani, C., Carollo, C. M., & Dekel, A. 2007, *MNRAS*, 375, 489
- Hahn, O., Teyssier, R., & Carollo, C. M. 2010, *MNRAS*, 405, 274
- Haynes, M. P., & Giovanelli, R. 1984, *AJ*, 89, 758

- Helou, G. 1984, *ApJ*, 284, 471
- Hirv, A., Pelt, J., Saar, E., et al. 2017, *A&A*, 599, A31
- Joachimi, B., Cacciato, M., Kitching, T. D., et al. 2015, *Space Sci. Rev.*, 193, 1
- Kim, S., Rey, S.-C., Bureau, M., et al. 2016, *ApJ*, 833, 207
- Laigle, C., Pichon, C., Codis, S., et al. 2015, *MNRAS*, 446, 2744
- Lee, J., & Pen, U.-L. 2000, *ApJ*, 532, L5
- Lee, J., & Pen, U.-L. 2001, *ApJ*, 555, 106
- Lee, J. 2004, *ApJ*, 614, L1
- Lee, J., & Erdogdu, P. 2007, *ApJ*, 671, 1248
- Lee, J., & Pen, U.-L. 2008, *ApJ*, 681, 798-805
- Lee, J. 2011, *ApJ*, 732, 99
- Libeskind, N. I., Hoffman, Y., Forero-Romero, J., et al. 2013, *MNRAS*, 428, 2489
- Navarro, J. F., Abadi, M. G., & Steinmetz, M. 2004, *ApJ*, 613, L41
- Peebles, P. J. E. 1969, *ApJ*, 155, 393
- Pen, U.-L., Lee, J., & Seljak, U. 2000, *ApJ*, 543, L107
- Porciani, C., Dekel, A., & Hoffman, Y. 2002, *MNRAS*, 332, 325
- Shandarin, S. F. 1994, *Physica D Nonlinear Phenomena*, 77, 342
- Shandarin, S. F., Melott, A. L., McDavitt, K., Pauls, J. L., & Tinker, J. 1995, *Physical Review Letters*, 75, 7
- Slosar, A., & White, M. 2009, *JCAP*, 6, 009
- Tempel, E., Stoica, R. S., & Saar, E. 2013, *MNRAS*, 428, 1827
- Tempel, E., & Libeskind, N. I. 2013, *ApJ*, 775, L42
- Tenneti, A., Mandelbaum, R., Di Matteo, T., Feng, Y., & Khandai, N. 2014, *MNRAS*, 441, 470
- Trujillo, I., Carretero, C., & Patiri, S. G. 2006, *ApJ*, 640, L111

- Varela, J., Betancort-Rijo, J., Trujillo, I., & Ricciardelli, E. 2012, *ApJ*, 744, 82
- Velliscig, M., Cacciato, M., Schaye, J., et al. 2015, *MNRAS*, 453, 721
- Welker, C., Devriendt, J., Dubois, Y., Pichon, C., & Peirani, S. 2014, *MNRAS*, 445, L46
- West, M. J., Jones, C., & Forman, W. 1995, *ApJ*, 451, L5
- White, S. D. M. 1984, *ApJ*, 286, 38
- Zel'dovich, Y. B. 1970, *A&A*, 5, 84
- Zhang, Y., Yang, X., Wang, H., et al. 2015, *ApJ*, 798, 17
- Zjupa, J., & Springel, V. 2017, *MNRAS*, 466, 1625

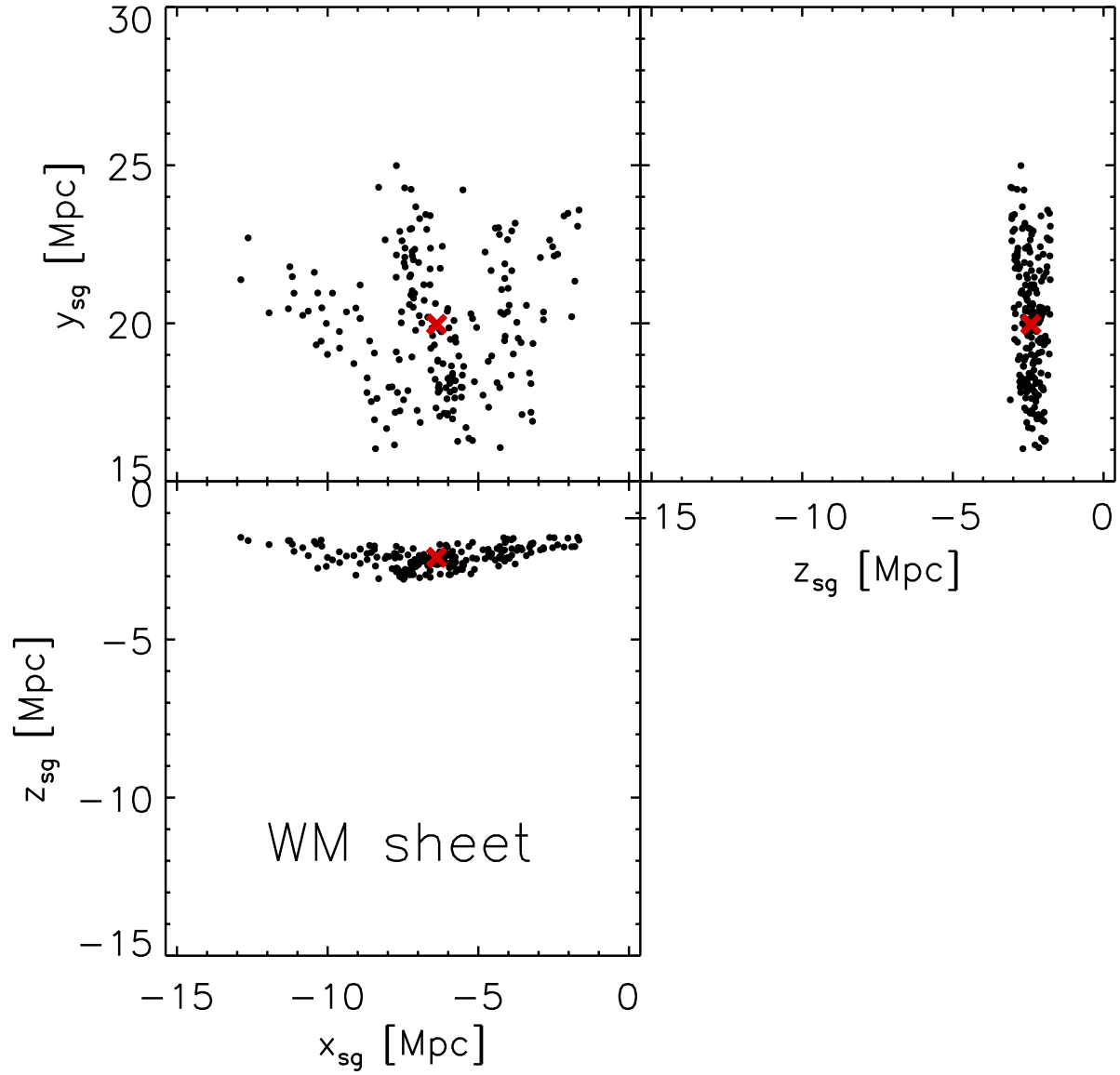


Fig. 1.— Configuration of the constituent galaxies of the WM sheet in the supergalactic coordinate system. The red cross in each panel represents the projected position of the center of the WM sheet.

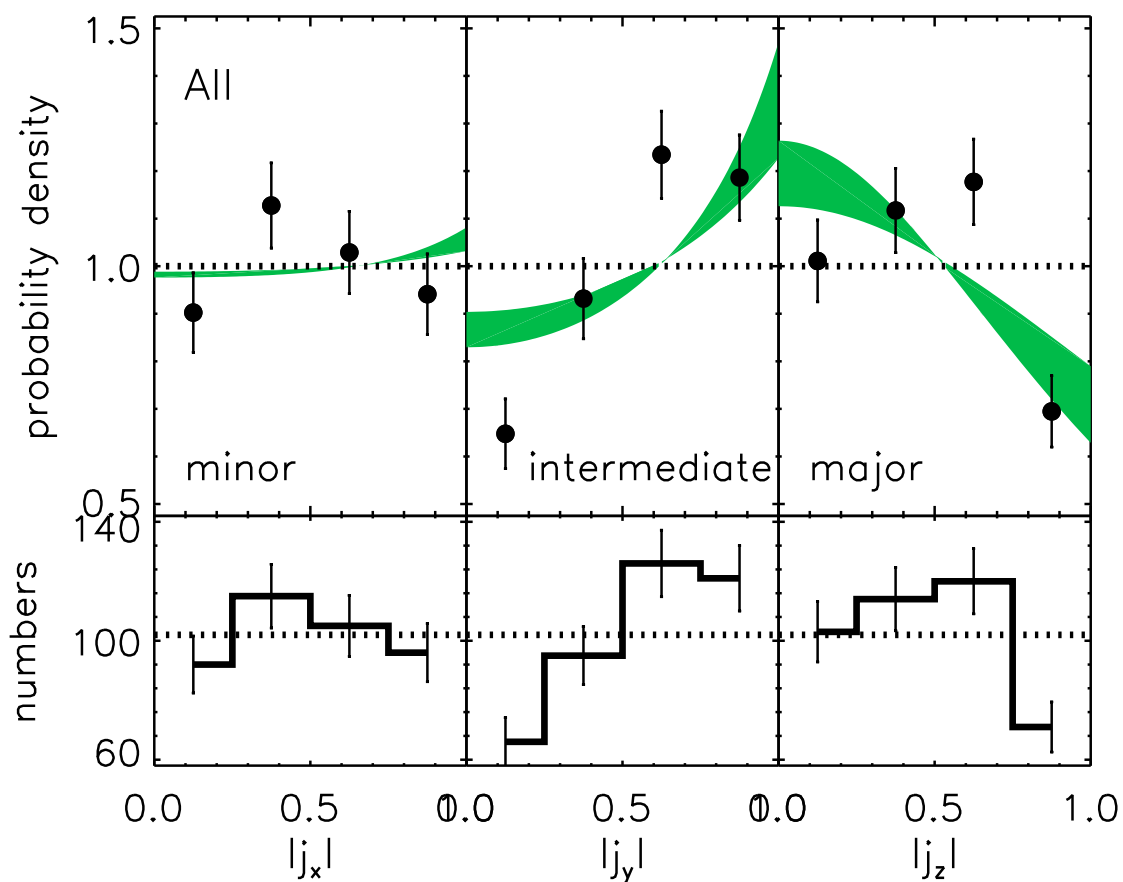


Fig. 2.— Probability density functions of the x , y and z -axis components of the unit spin vectors, \mathbf{j} , of all WMs galaxies are displayed as filled circular dots with the bootstrap errors in the top-left, top-middle and top-right panels, respectively. In each top panel, the green area corresponds to the theoretical prediction of the LTT model. The corresponding distributions of the realization numbers are also shown as histograms with the Poisson errors in the bottom panels.

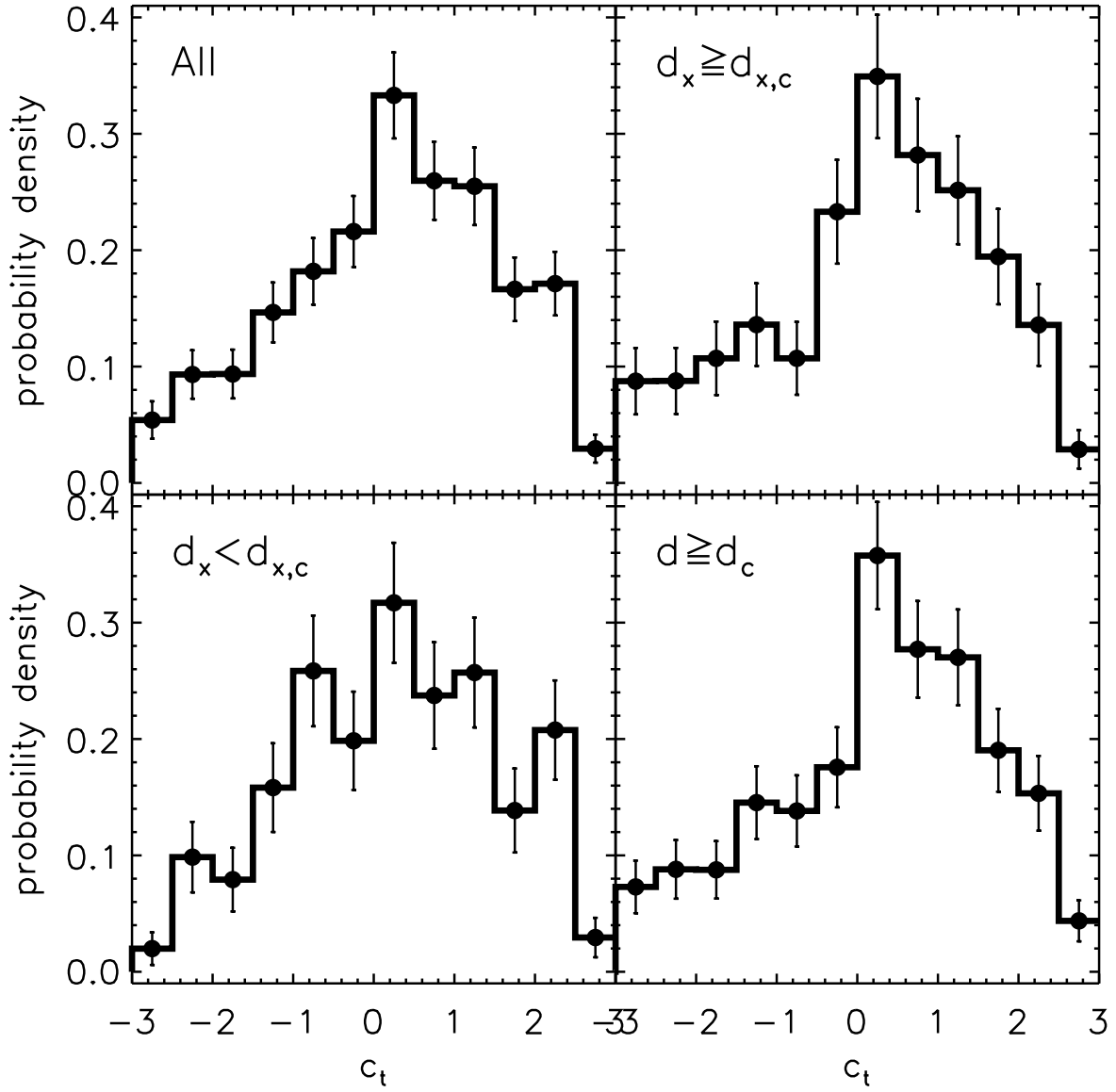


Fig. 3.— Probability density functions of the tidal link parameters c_t .

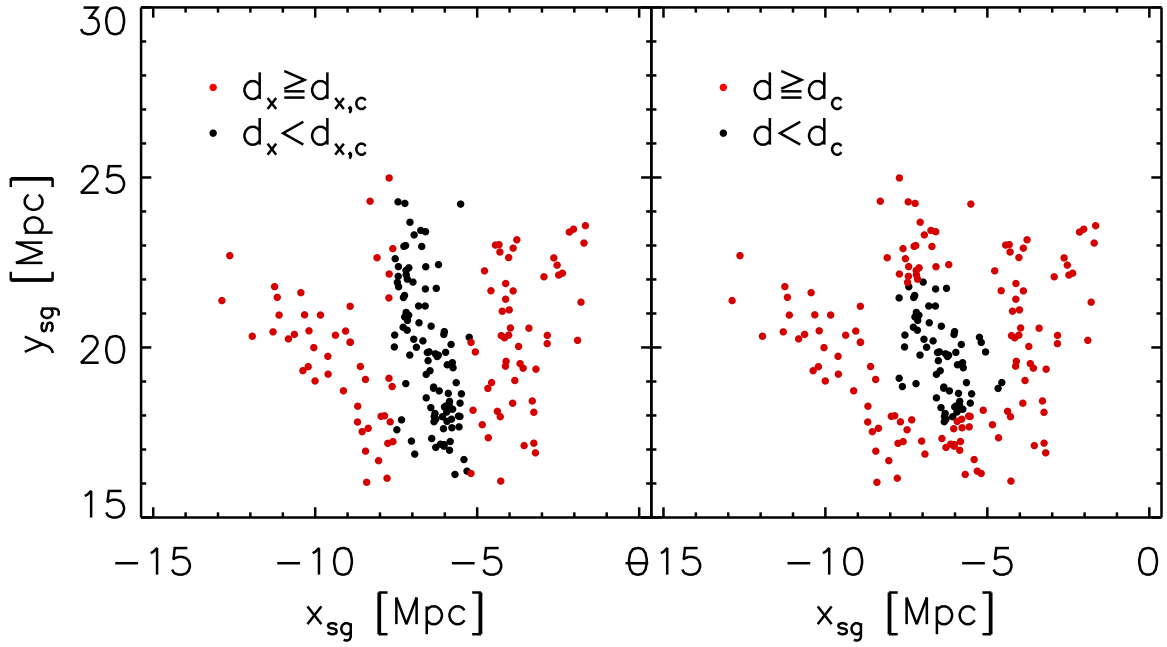


Fig. 4.— Configuration of the WM galaxies with $d_x > d_{x,c}$ (left panel) and with $d > d_c$ (right panel) as filled red dots in the supergalactic plane. In each panel, the configuration of the other WM galaxies are also shown as filled black dots.

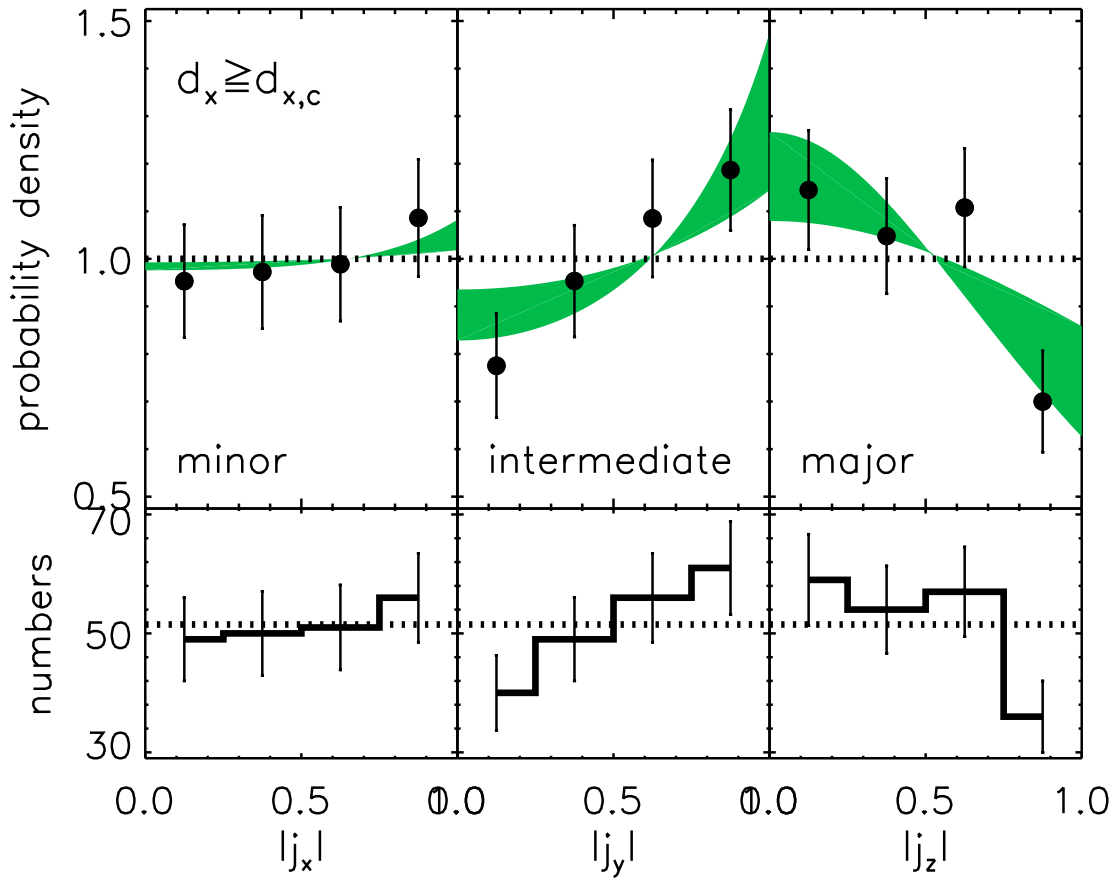


Fig. 5.— Same as Figure 2 but for the case of those WMs galaxies satisfying $d_x \geq d_{x,c}$.

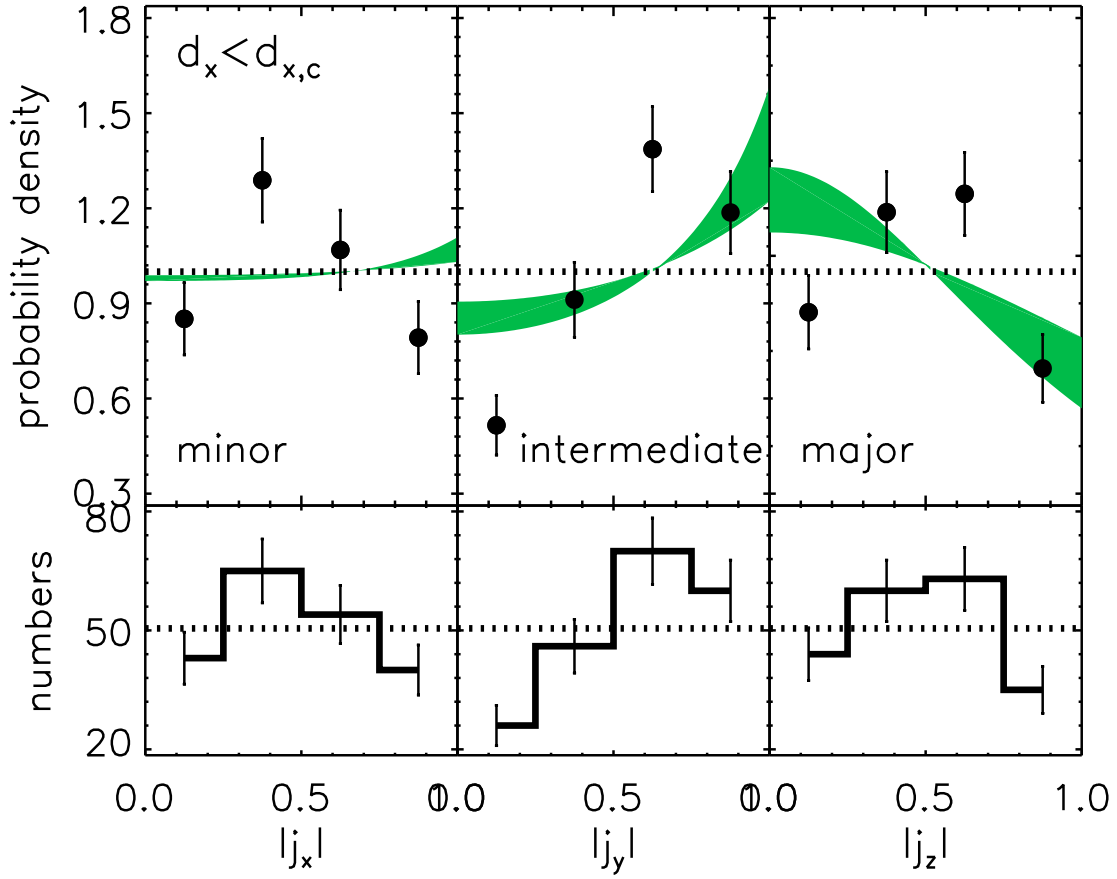


Fig. 6.— Same as Figure 2 but for the case of those WMs galaxies satisfying $d_x < d_{x,c}$.

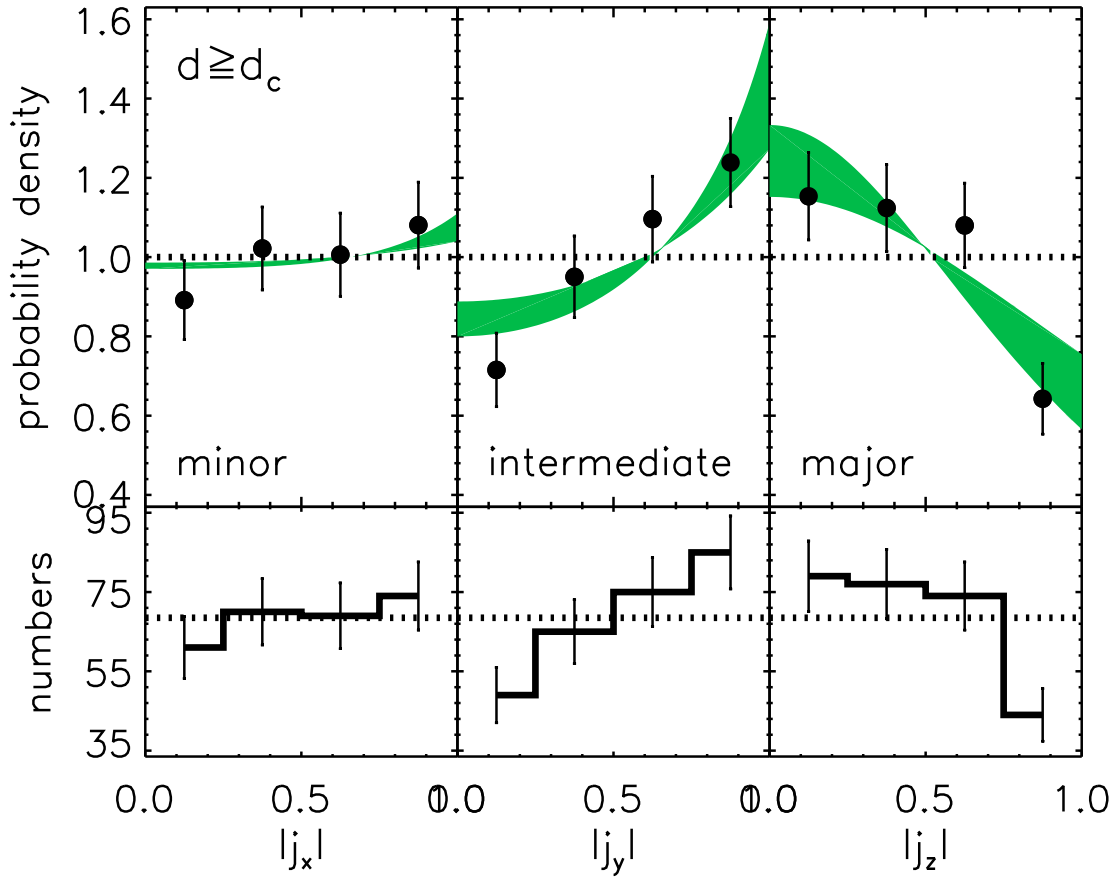


Fig. 7.— Same as Figure 2 but for the case of those WMs galaxies satisfying $d \geq d_c$.

Table 1. Spatial extents of the WMs galaxies

x_{sg} (Mpc)	y_{sg} (Mpc)	z_{sg} (Mpc)
$[-12.88, -1.66]$	$[16.03, 24.99]$	$[-3.10, -1.77]$

Table 2. Tidal link parameters and their errors.

constraint	N_r	\bar{c}_t	σ_{c_t}
none	408	0.24	0.07
$d_x \geq d_{x,c}$	206	0.21	0.10
$d_x < d_{x,c}$	202	0.27	0.11
$d \geq d_c$	274	0.29	0.09